Supplementary information

Cohesive Co and Mo_2C Heterostructure Catalysts Strongly Confined to Hollow Carbon Support for Enhanced Kinetics and Durability in the Alkaline Hydrogen Evolution Reaction

Hyein Lee,‡[a] Miyeon Kim,‡[b] Jeonghan Roh,[a] KwangHo Lee,[a] Jooyoung Shin,[c] Jeong Woo Han,*[b] MinJoong Kim,*[d] and EunAe Cho*[a]

[a]Department of Materials Science and Engineering, KAIST, 291 Daehak-ro, Yuseong-gu, Daejeon 34141, Republic of Korea.

[b]Department of Materials Science and Engineering, Research Institute of Advanced Materials, Seoul National University, Seoul 08826, Republic of Korea.

[c]Hydrogen Research Department, Korea Institute of Energy Research, 152 Gajeong-ro, Yuseong-gu, Daejeon, 34129 Republic of Korea.

[d]Department of Materials Science and Engineering, Kyung Hee University, 1732 Deogyeong-daero, Yongin, Gyeonggi-do 17104, Republic of Korea.

*Corresponding Author: eacho@kaist.ac.kr (EunAe Cho), mj.kim@khu.ac.kr (MinJoong Kim), jwhan98@snu.ac.kr (Jeong Woo Han)

‡H. L. and M. K. contributed equally to this paper.

Keyword: Alkaline hydrogen evolution reaction, N-doped carbon hollow polyhedron, Cobalt, Molybdenum carbide, Dual-active sites

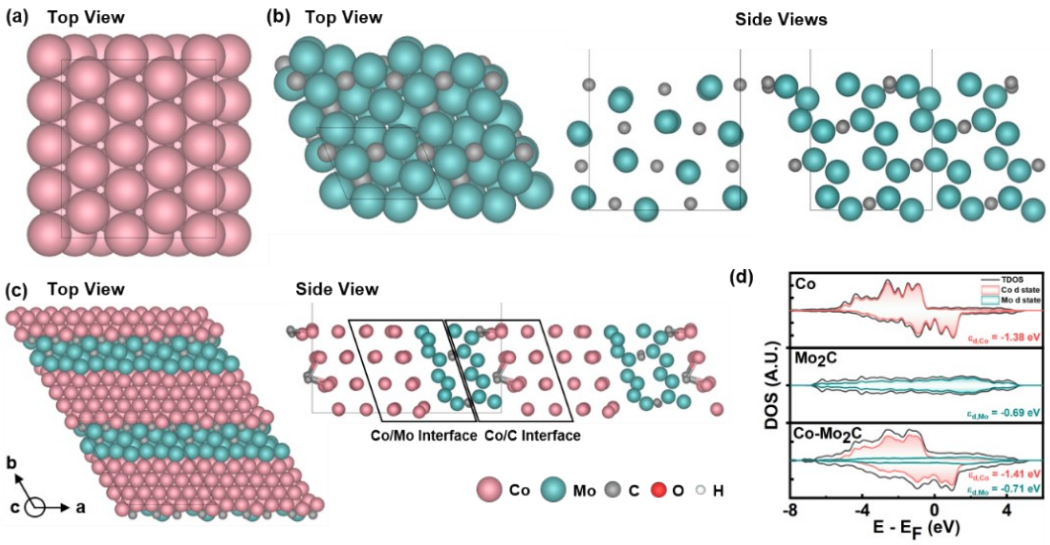

Figure S1. DFT models of (a) Co FCC (111), (b) Mo_2C (101), and (c) Co-Mo_2C. (d) Density of States (DOS) of Co, Mo_2C, and Co-Mo_2C models.

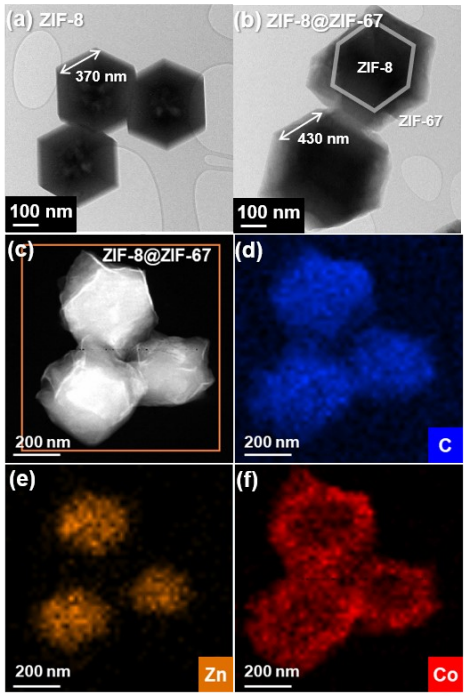

Figure S2. TEM images of (a) ZIF-8 and (b) ZIF-8@ZIF-67. HAADF-STEM elemental mapping of (c-f) ZIF-8@ZIF-67.

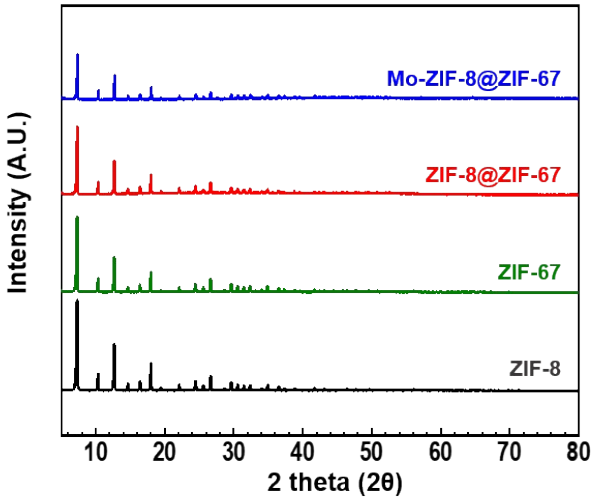

Figure S3. XRD patterns of ZIF-8, ZIF-67, ZIF-8@ZIF-67, and Mo-ZIF-8@ZIF-67.

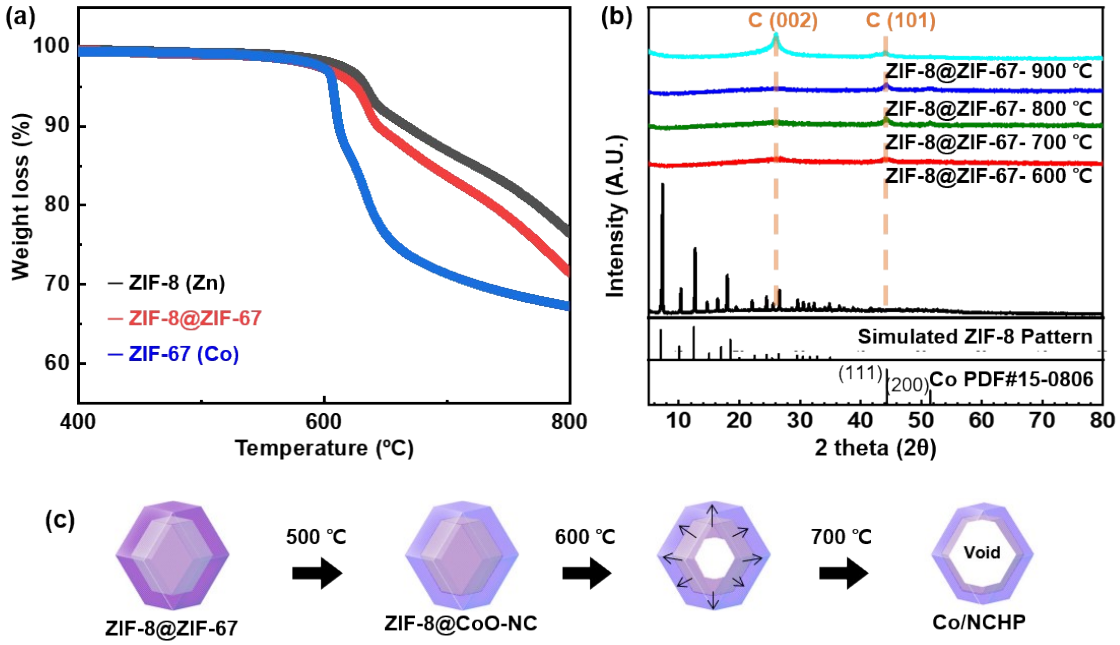

Figure S4. (a) TGA analysis of ZIF-8, ZIF-8@ZIF-67, and ZIF-67 under N_2, heated from 30 to 805 °C at 10 K·min^{-1}. (b) XRD patterns of ZIF-8@ZIF-67 after thermal decomposition at various temperatures. (c) Schematic representation of the thermal decomposition process of ZIF-8@ZIF-67.

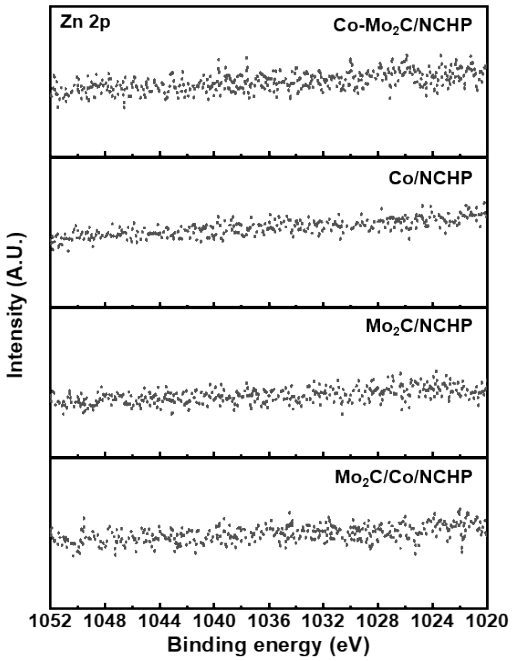

Figure S5. XPS spectra of Zn 2p of Co-Mo_2C/NCHP, Co/NCHP, Mo_2C/NCHP, and Mo_2C/Co/NCHP.

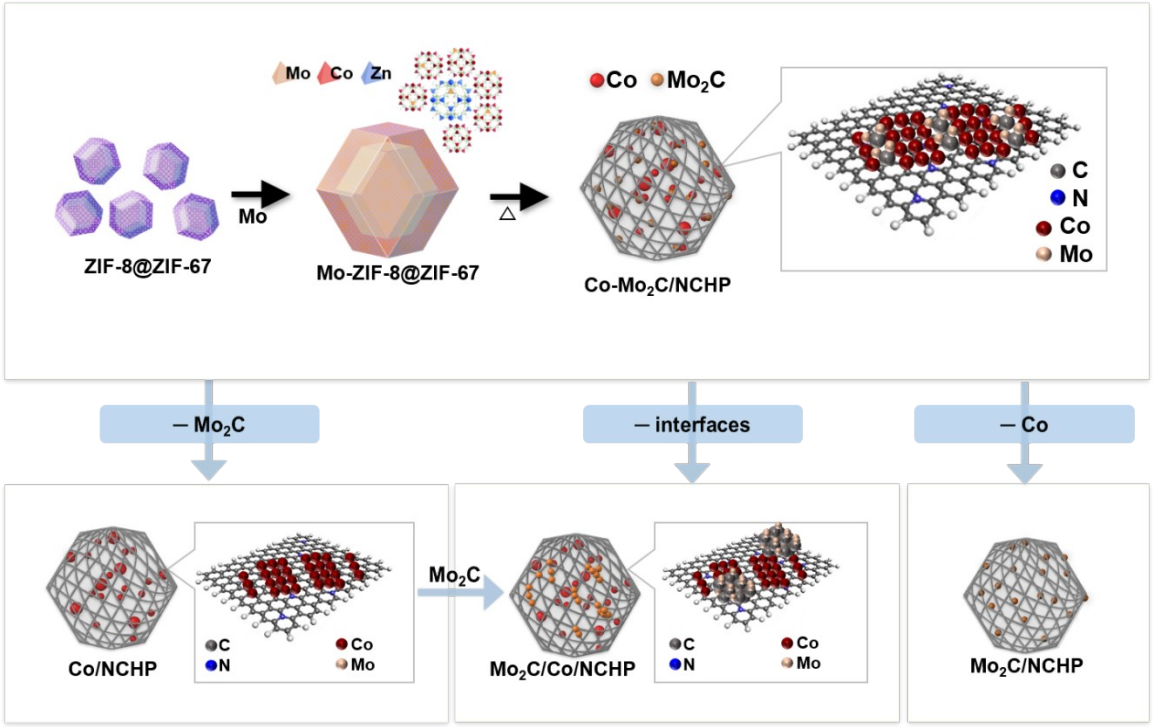

Figure S6. Schematic illustration of the preparation of Co/NCHP, Mo_2C/NCHP, Mo_2C/Co/NCHP, and Co-Mo_2C/NCHP.

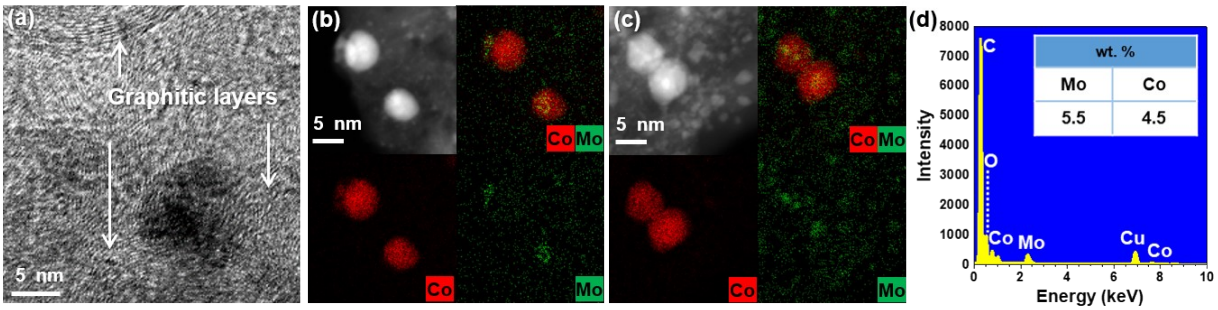

Figure S7. (a) HRTEM image, (b, c) HAADF-STEM elemental mapping results, and (d) typical EDX spectrum of Co-Mo_2C/NCHP.

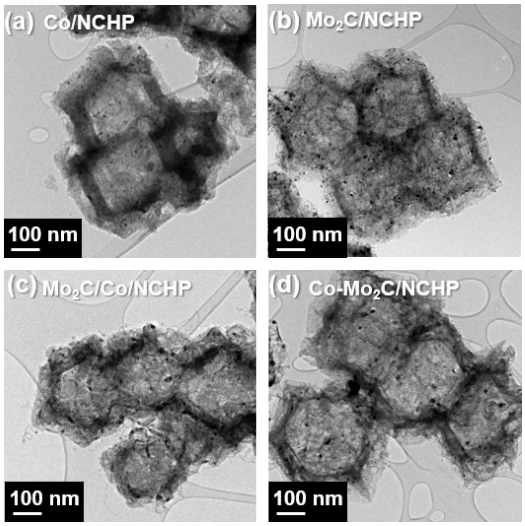

Figure S8. TEM images of (a) Co/NCHP, (b) Mo_2C/NCHP, (c) Mo_2C/Co/NCHP, and (d) Co-Mo_2C/NCHP.

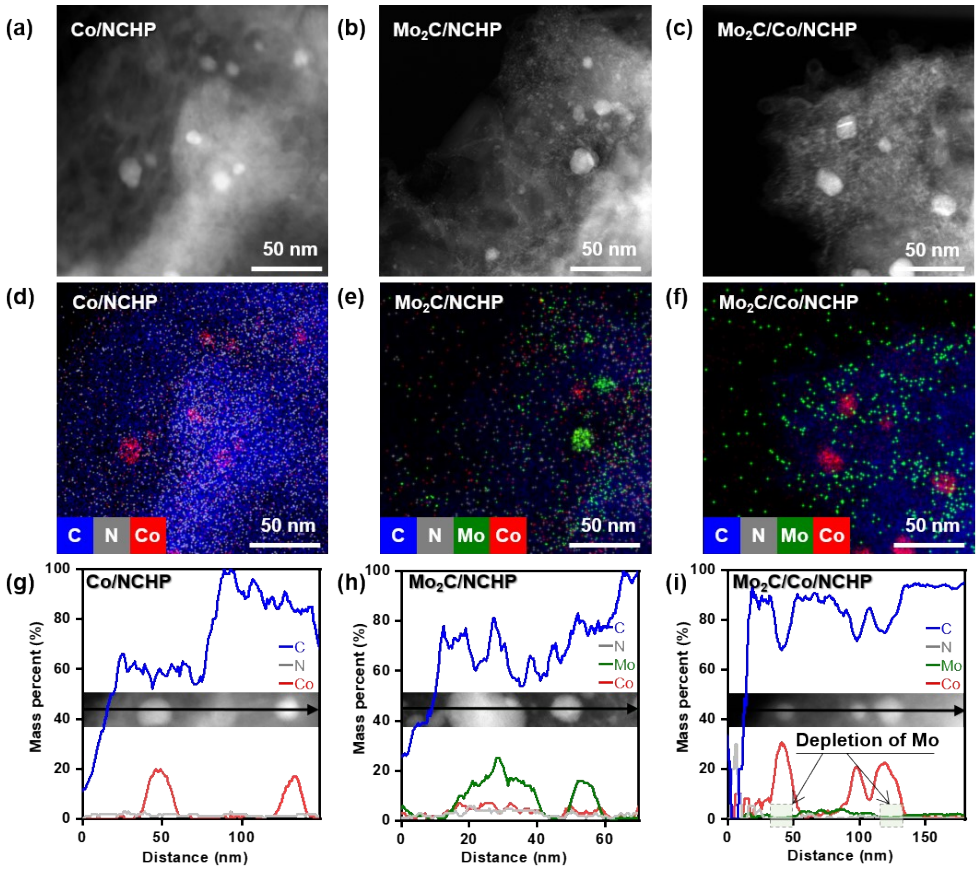

Figure S9. (a-c) HAADF-STEM images, (d-f) elemental mapping, and (g-i) elemental line scanning results of Co/NCHP, Mo_2C/NCHP, and Mo_2C/Co/NCHP.

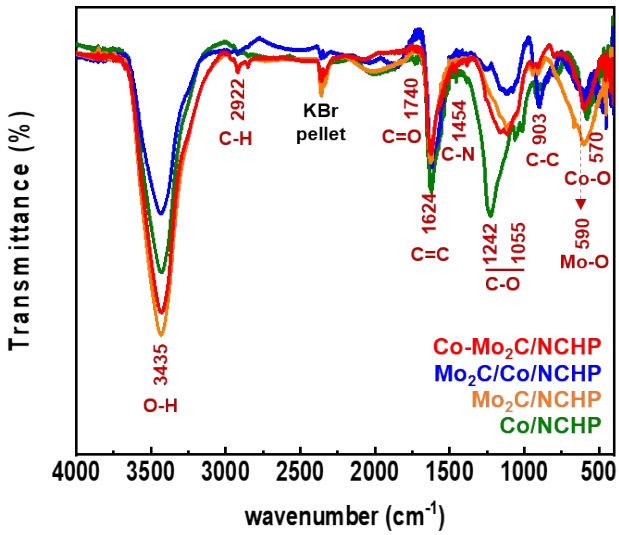

Figure S10. FT-IR spectra of Co/NCHP, Mo_2C/NCHP, Mo_2C/Co/NCHP, and Co-Mo_2C/NCHP.

Table S1. The best EXAFS fitting parameters for Co foil, Co-Mo_2C/NCHP, Co/NCHP, Mo_2C/Co/NCHP, CoO, Co_3O_4.

Catalyst	Shell	CN[a]	R (Å)	σ^2(Å^2)	ΔE_0(eV)	R factor
Co foil[b]	Co-Co	12	2.49	0.006	8.2	0.001
Co-Mo_2C/NCHP[b]	Co-Co	10	2.42	0.006	7.8	0.001
	Co-Mo	0.5	2.56	0.008		
Co/NCHP[b]	Co-Co	8.1	2.50	0.007	-4.2	0.008
	Co-O	0.7	1.89	0.008		
Mo_2C/Co/NCHP[b]	Co-Co	6.4	2.50	0.005		0.005
	Co-O	0.9	1.97	0.009		
Commercial CoO[b]	Co-Co	10.8	3.00	0.008	-2.8	0.007
	Co-O	4.5	2.07	0.009		
Commercial Co_3O_4[b]	Co-Co1	6.7	2.90	0.005	-5.0	0.004
	Co-Co2	5.5	3.34	0.008		
	Co-O	4.9	1.92	0.003		

[a]N, coordination number; σ^2, Debye-Waller factor to account for both thermal and structural disorders; ΔE_0, inner potential correction; R, R factor indicating the goodness of the fit. Error bounds (accuracies) that characterize the structural parameters obtained by EXAFS spectroscopy are estimated as N ± 20%; R ± 1%; σ^2 ± 20%; E_0 ± 20%. S_0^2 is fixed to 0.77 as determined from Co foil fitting. Bold numbers indicate fixed coordination number (N) according to the crystal structure. Co-Co1 and Co-Co2 represent the first and second nearest Co atoms to the central Co atom. [b]Fitting range: 3.0 ≤ k (/Å) ≤ 11 and 1.3 ≤ R (Å) ≤ 3.5.

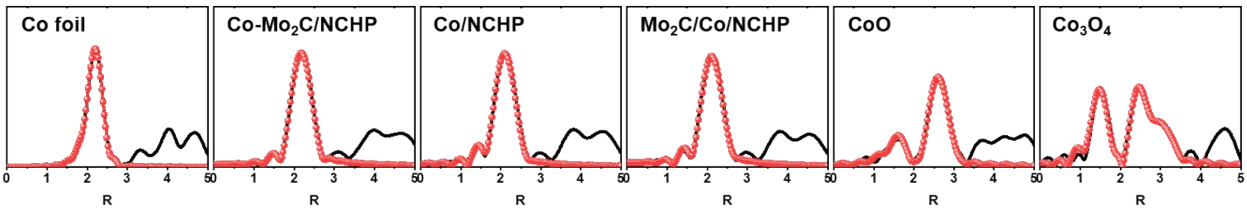

Figure S11. EXAFS fitting spectra for (a) Co foil, (b) Co-Mo_2C/NCHP, (c) Co/NCHP, (d) Mo_2C/Co/NCHP, (e) CoO and (f) Co_3O_4. The corresponding fitting parameters are listed in Table S1.

Table S2. The best EXAFS fitting parameters for Mo foil, Co-Mo_2C/NCHP, Mo_2C, Mo_2C/NCHP, Mo_2C/Co/NCHP, MoO_3.

Catalyst	Shell	CN[a]	R(Å)	σ^2(Å^2)	ΔE_0(eV)	R factor
Mo foil[b]	Mo-Mo1	8	2.72	0.003	-7.1	0.003
	Mo-Mo2	6	3.14	0.003		
Co-Mo_2C/NCHP[b]	Mo-Mo1	5.3	2.98	0.006	-7.8	0.007
	Mo-Co	0.5	2.68	0.009		
	Mo-C	1.8	2.1	0.001		
Commercial Mo_2C[c]	Mo-Mo1	2.5	2.89	0.001	5.0	0.005
	Mo-Mo2	1.0	3.00	0.001		
	Mo-C	2.3	2.06	0.009		
Mo_2C/NCHP[b]	Mo-Mo1	3.4	2.53	0.007	1.3	0.009
	Mo-Mo2	0.3	2.97	0.006		
	Mo-C	1.7	1.89	0.009		

	Mo-Mo1	0.7	2.71	0.010		
	Mo-Mo2	1.8	2.99	0.007		
Mo_2C/Co/NCHP[d]					7.3	0.009
	Mo-C	1.2	2.02	0.001		
	Mo-O	0.9	1.75	0.001		
	Mo-O1	0.6	1.65	0.003		
Commercial MoO_3[d]	Mo-O2	1.2	1.96	0.001	-7.2	0.008
	Mo-O3	0.9	2.11	0.001		

[a]N, coordination number; σ^2, Debye-Waller factor to account for both thermal and structural disorders; ΔE_0, inner potential correction; R, R factor indicating the goodness of the fit. Error bounds (accuracies) that characterize the structural parameters obtained by EXAFS spectroscopy are estimated as N ± 20%; R ± 1%; σ^2 ± 20%; E_0 ± 20%. S_0^2 is fixed to 0.93 as determined from Mo foil fitting. Bold numbers indicate fixed coordination number (N) according to the crystal structure. Mo-Mo1 and Mo-Mo2 represent the first and second nearest Mo atoms to the central Mo atom. Similarly, O1, O2, and O3 represent the first, second, and third nearest neighbor coordination O atoms. [b]Fitting range: 3.2 ≤ k (/Å) ≤ 15.7 and 2.0 ≤ R (Å) ≤ 3.1. [c]Fitting range: 3.1 ≤ k (/Å) ≤ 15.7 and 1.5 ≤ R (Å) ≤ 3.3. [d]Fitting range: 3.0 ≤ k (/Å) ≤ 12.5 and 1.2 ≤ R (Å) ≤ 2.2.

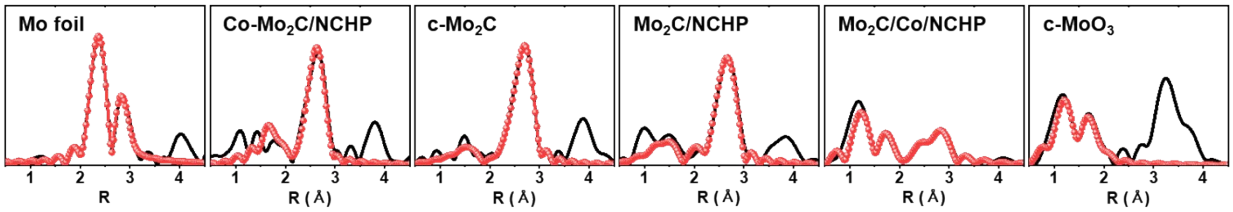

Figure S12. EXAFS fitting spectra for (a) Mo foil, (b) Co-Mo_2C/NCHP, (c) Mo_2C, (d) Mo_2C/NCHP, (e) Mo_2C/Co/NCHP, and (f) MoO_3. The corresponding fitting parameters are listed in Table S2.

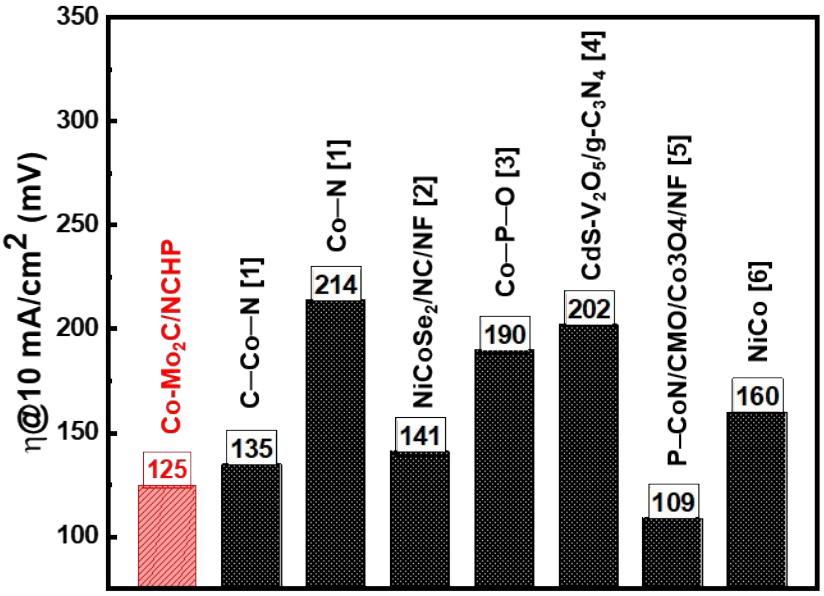

Figure S13. Comparison of the cell voltages required to achieve 10 mA/cm^2 of Co-Mo_2C/NCHP in 1 M KOH using different alkaline water electrolyzers.[1-6]

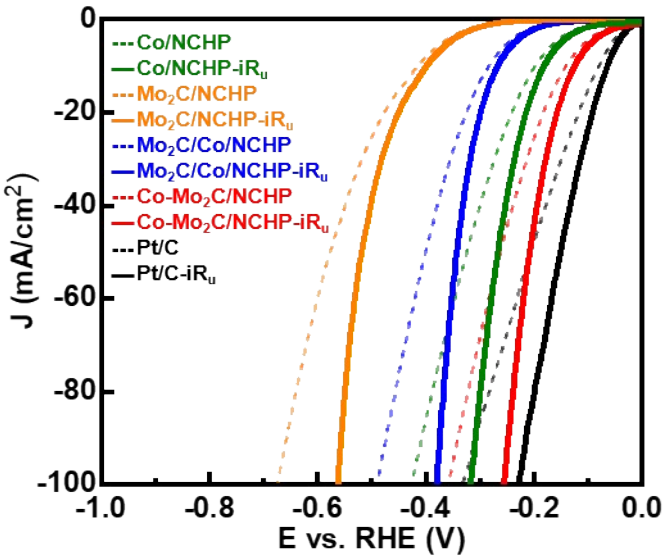

Figure S14. HER polarization curves at a scan rate of 0.05 V/s in 1.0 M KOH.

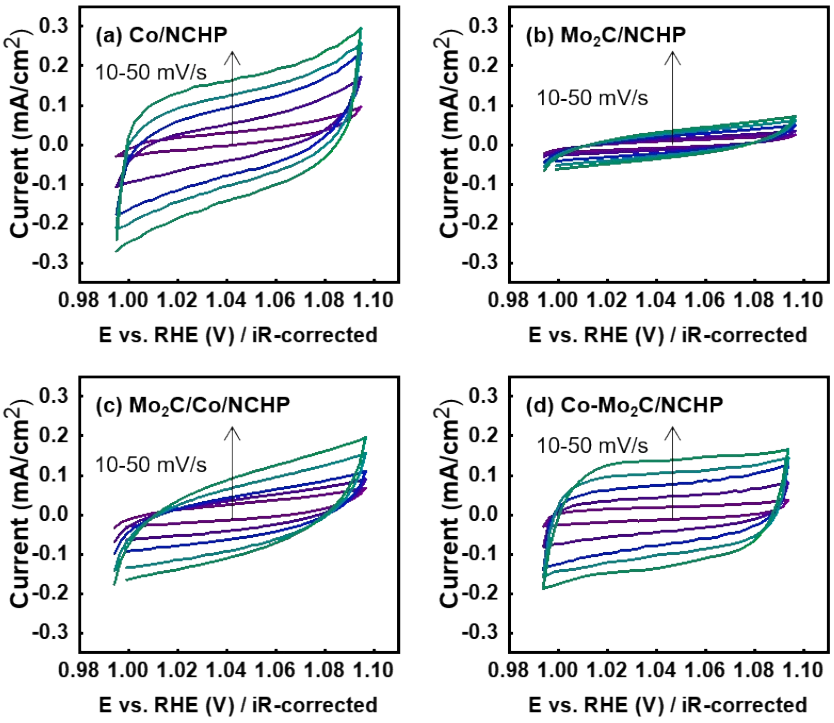

Figure S15. Cyclic voltammograms of (a) Co/NCHP, (b) Mo_2C/NCHP, (c) Mo_2C/Co/NCHP, and (d) Co-Mo_2C/NCHP, recorded in potential region between 1.0 and 1.1 V_{RHE} at scan rates ranging from 10 to 50 mV/s in H_2-saturated 1 M KOH solution.

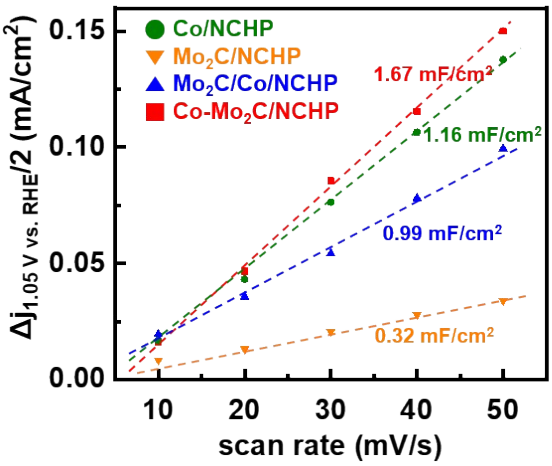

Figure S16. Scan rate dependence of the capacitive current densities for Co/NCHP, Mo_2C/NCHP, Mo_2C/Co/NCHP, and Co-Mo_2C/NCHP. The capacitive current densities are the sum of the anodic and cathodic current densities at 1.05 V_{RHE}, derived from the data in Figure S15.

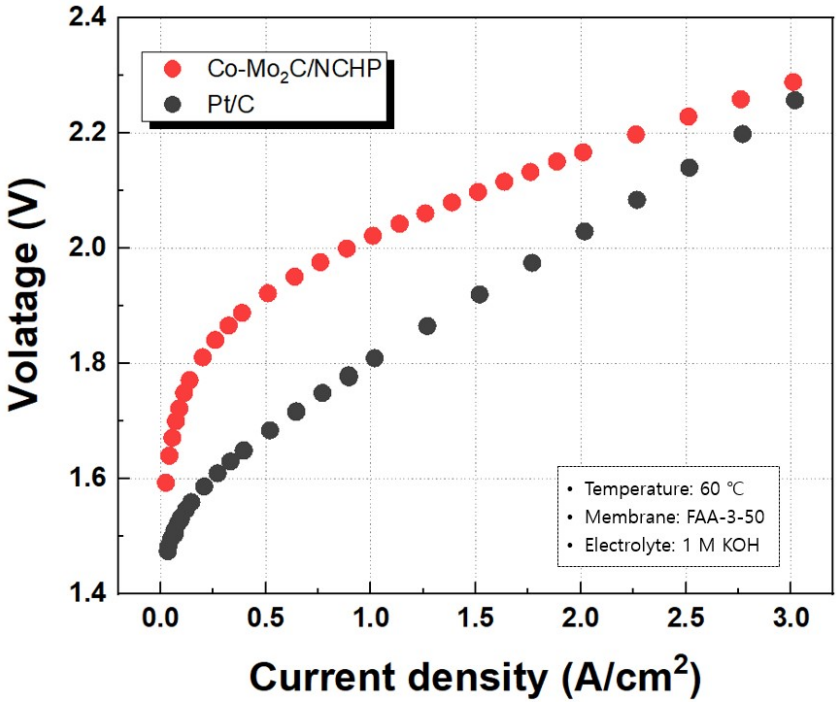

Figure S17. Anion exchange membrane water electrolysis single-cell performance of Co-Mo_2C/NCHP and Pt/C cathode with IrO_2 anode.

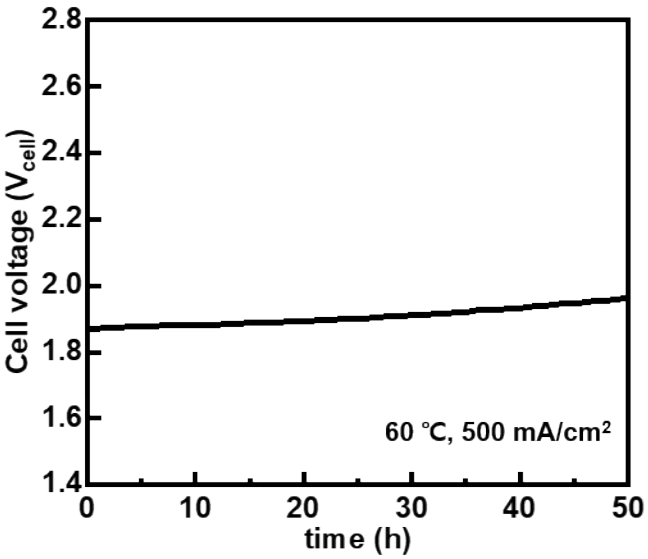

Figure S18. Chronopotentiometry results measured at a current density of 0.5 A/cm^2 of the AEMWE single cells using Co-Mo_2C/NCHP as anode catalysts.

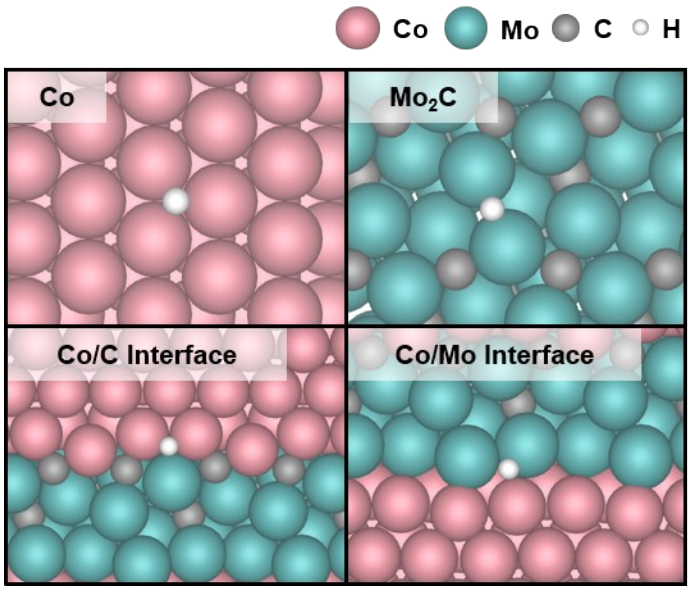

Figure S19. The results of H adsorption on individual Co and Mo_2C models and on the Co/C interface and the Co/Mo interface in Co-Mo_2C heterostructure.

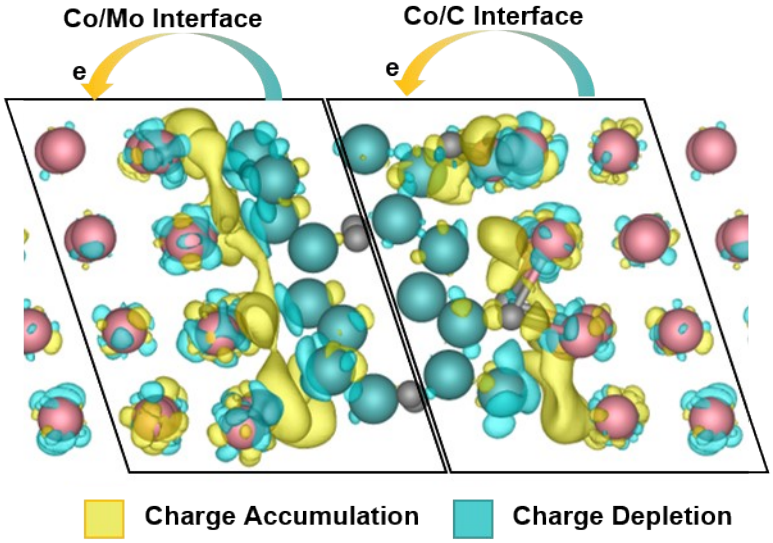

Figure S20. The charge density difference of Co-Mo_2C, divided by the Co/Mo interface and the Co/C interface. The iso-surface level is set as 0.01 e/$Å^3$.

Table S3. The charge density difference in the Co-Mo_2C model.

Charge Density Difference	Co	Mo	C
Co/C Interface	+2.22 e	-0.65 e	-1.45 e
Co/Mo Interface	-2.47 e	+2.65 e	-0.18 e
Total	-0.25 e	+1.99 e	-1.74 e

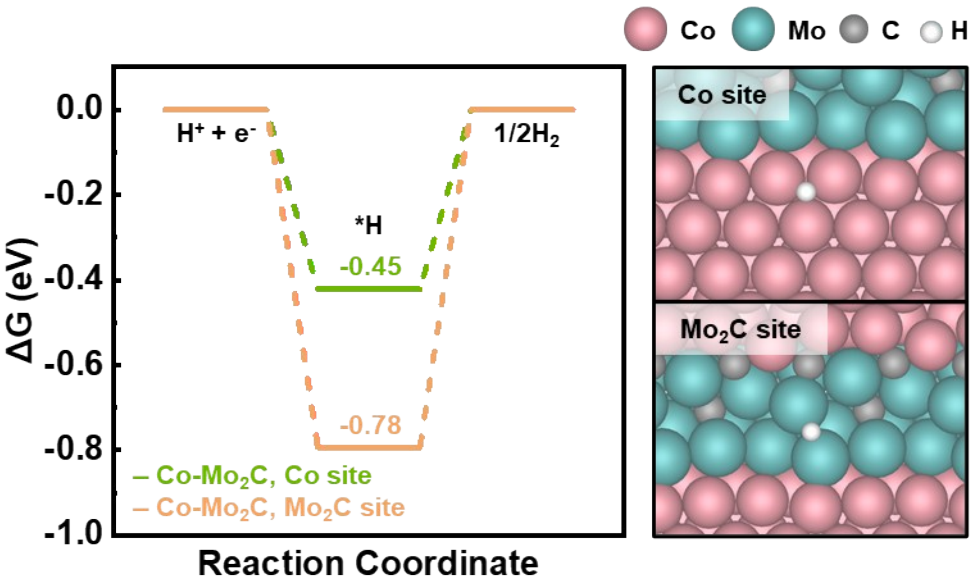

Figure S21. The Gibbs free energy of H adsorption on the Co site and the Mo_2C site in Co-Mo_2C heterostructure.

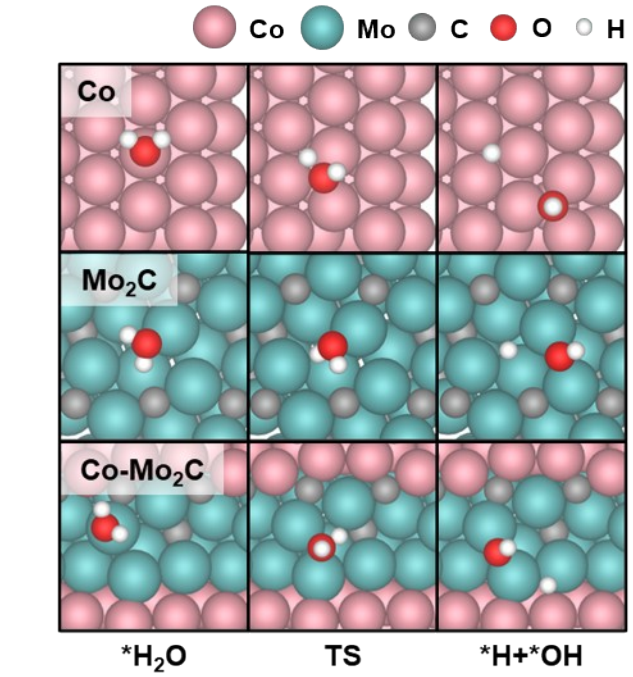

Figure S22. The results of water dissociation mechanisms on individual Co and Mo_2C models and on Co-Mo_2C heterostructure.

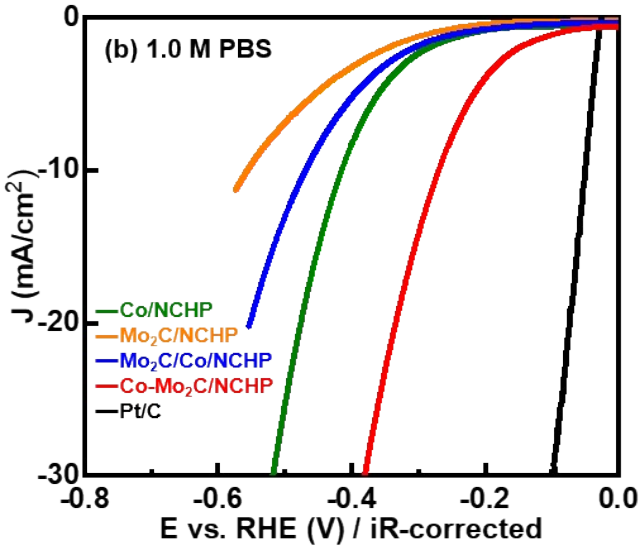

Figure S23. IR-corrected HER polarization curves at a scan rate of 0.05 V/s in 1.0 M PBS.

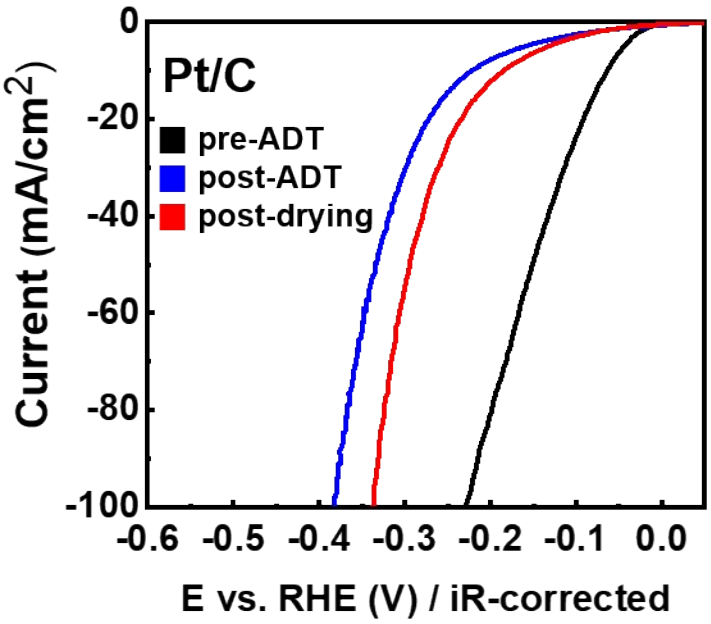

Figure S24. IR-corrected HER polarization curves of Pt/C.

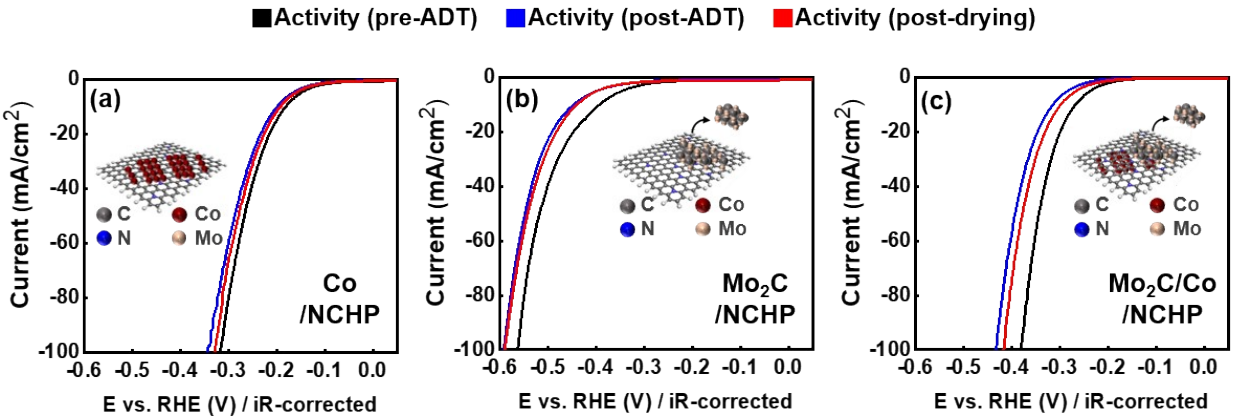

Figure S25. IR-corrected HER polarization curves of (a) Co/NCHP, (b) Mo_2C/NCHP, and (c) Mo_2C/Co/NCHP.

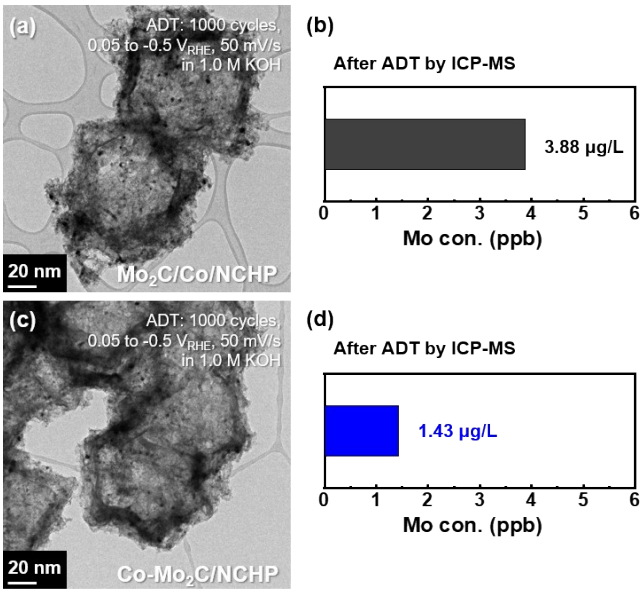

Figure S26. TEM images after 1000 potential cycles and Mo concentration determined by ICP for (a-b) Mo_2C/Co/NCHP and (c-d) Co-Mo_2C/NCHP.

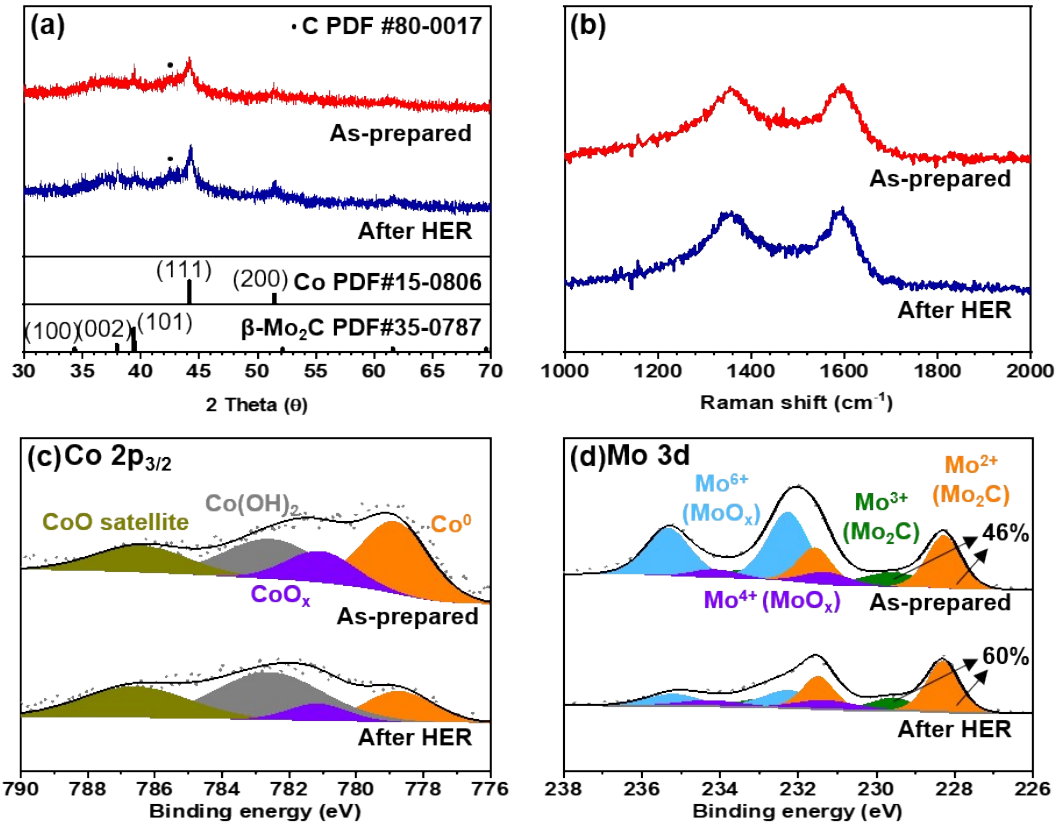

Figure S27. (a) XRD patterns, (b) Raman spectra, (c) Co $2p_{3/2}$ XPS spectra, and (d) Mo 3d spectra of Co-Mo_2C/NCHP before and after 1000 HER potential cycles.

References

1. S. Radhakrishnan, S. Ramakrishnan, S. K. Jayaraj, M. Mamlouk, B.-S. Kim, A Simple and Efficient Non-Noble Cathode Catalyst Based on Carbon Hollow Nanocapsules Containing Cobalt-Based Materials for Anion Exchange Membrane Water Electrolyzer, *small*, 2025, **21**, 2411019, DOI: 10.1002/smll.202411019.

2. X. Wang, C. Sun, Y. Zhang, W. Xin, X. Jiang, Z. Lu, L. Yu, M. Zhu, L. Yang, Discrepancy of alkaline/neutral hydrogen evolution activity from $NiCoSe_2$/NC and Co–NiSe/NC derived from in-

situ thermal and solution processing selenizations of ZIF-67, *Int. J. Hydrogen Energy*, 2024, **49**, 1236-1244, DOI: 10.1016/j.ijhydene.2023.09.155.

3. P. J. Sharma, S. Siraj, P. Sahatiya, C.K. Sumesh, P. M. Pataniya, Electroless plating of Co–P–O electrocatalyst on carbon cloth for alkaline water electrolysis, *J. Electroanal. Chem.*, 2024, **967**, 118491, DOI: 10.1016/j.jelechem.2024.118491.

4. T. Munawar, A. Bashir, F. Iqbal, M. Rafaqat, C. Guo, M. Zhiani, C. Zhao, Y. Tong, S. A. Khan, M. Koc, C.-F. Yan, g-C_3N_4-modulated CdS-V_2O_5/g-C_3N_4 nanosheets as efficient alkaline OER and HER electrocatalyst for water-splitting, *Fuel*, 2025, **385**, 134100, DOI: 10.1016/j.fuel.2024.134100.

5. J. Ran, Z. Zhang, H. Feng, H. Zhao, D.F. Chai, X. Huang, W. Zhang, M. Zhao, G. Dong, Y. Zang, P-doped Co-based nanoarray heterojunction with multi-interfaces for complementary HER/OER electrocatalysts towards high-efficiency overall water splitting in alkaline, *Int. J. Hydrogen Energy*, 2024, **64**, 935-946, DOI: 10.1016/j.ijhydene.2024.03.330.

6. Y. Sun, Z. Li, F. Zhu, F. Yin, S. Ge, F. F. Yang, L. Gao, G. Chen, F. Yang, P. Hu, Chemical Coprecipitation-Thermal Synthesis of Nano-Ni-Co Alloy for Efficient Hydrogen and Oxygen Evolution Reactions, *Electrocatalysis*, 2024, **16**, 96-105, DOI: 10.1007/s12678-024-00902-w.